

Journal of Materials Chemistry C

Accepted Manuscript



This is an *Accepted Manuscript*, which has been through the Royal Society of Chemistry peer review process and has been accepted for publication.

Accepted Manuscripts are published online shortly after acceptance, before technical editing, formatting and proof reading. Using this free service, authors can make their results available to the community, in citable form, before we publish the edited article. We will replace this *Accepted Manuscript* with the edited and formatted *Advance Article* as soon as it is available.

You can find more information about *Accepted Manuscripts* in the [Information for Authors](#).

Please note that technical editing may introduce minor changes to the text and/or graphics, which may alter content. The journal's standard [Terms & Conditions](#) and the [Ethical guidelines](#) still apply. In no event shall the Royal Society of Chemistry be held responsible for any errors or omissions in this *Accepted Manuscript* or any consequences arising from the use of any information it contains.



Flexible ultraviolet photodetector based on single crystalline MoO₃ nanosheet

Qinghong Zheng,^{*a} Jin Huang,^b Shilin Cao,^a and Haili Gao^a

Received 00th January 20xx,
Accepted 00th January 20xx

DOI: 10.1039/x0xx00000x

www.rsc.org/

Large scale two dimensional orthorhombic structure MoO₃ single crystalline belts with bandgap of 3.28 eV were prepared by substrate-free physical vapor deposition. Ultra-thin MoO₃ nanosheets were exfoliated from the belt and transferred to a polyethylene terephthalate substrate. A flexible ultraviolet photodetector (UVPD) based on the single crystalline MoO₃ nanosheet was fabricated, and its optoelectronic response properties were investigated in detail. The UVPD has a high responsivity of 183 mA W⁻¹, a high on/off ratio of over two orders and a response speed of below 1 s. Moreover, the flexible UVPD exhibits excellent stability and reproducibility under different mechanical deformations. The excellent operating characteristics make the UVPD a potential candidate for wearable UV meters, touch sensor panels, communication devices and UV image cameras.

Introduction

Ultraviolet photodetectors (UVPDs) have attracted much attention for their broadening applications in ultraviolet environmental monitoring, biological analysis, and fire alarm.¹⁻³ Benefiting from large aspect ratio, high crystalline quality and unique optoelectronic properties, semiconductor nanostructures are acknowledged to be the most promising candidates for fabricating photodetectors with superior responsivity and fast response speed.^{4, 5} Dunn group developed a self-powered ZnO-nanorod based UVPD with a rapid decay time of 6.7 μs.⁶ Lee group reported a Graphene-ZnO Nanorod Hybrid UVPD, showing a high responsivity up to 3 × 10⁵ AW⁻¹.⁷

Flexible photodetectors with bending and torsion characteristics can extend their application range to wearable devices and biological tissues implantable devices.⁸⁻¹⁰ Two dimensional (2D) nanostructures are particularly suitable for flexible optoelectronic device. Compared to quantum dots and one-dimensional materials, 2D materials possess higher flexibility and carrier mobility, and are more compatible with commercial micro-manufacturing techniques.¹¹ Recently, 2D ultra-thin nanosheet semiconductors such as WS₂,¹² MoS₂,^{13, 14} and GaSe¹⁵ have been researched extensively for their potential applications in photodetectors. The ultra-thin WS₂ based photodetector showed a responsivity of 0.092 mA W⁻¹ and fast response speed of 5.3 ms. A transistor type photodetector with responsivity of 7.5 mA W⁻¹ was demonstrated using MoS₂ channel.

However, these reported photodetectors were mainly fabricated based on narrow bandgap 2D semiconductor materials, thus lack of UV spectral selectivity. To achieve the selective performance in the UV region, optical filters were needed for the photodetector devices to remove the visible light. The filters can also reduce the light intensity and hence lower the optical response. An alternative way to realize UV detection is fabricating the UVPD based on wide bandgap semiconductor. So far, there are few reports regarding flexible UVPD made of wide bandgap 2D semiconductor nanosheet¹¹. Among the 2D semiconductor materials, orthorhombic structure molybdenum trioxide (α-MoO₃) is of special interest

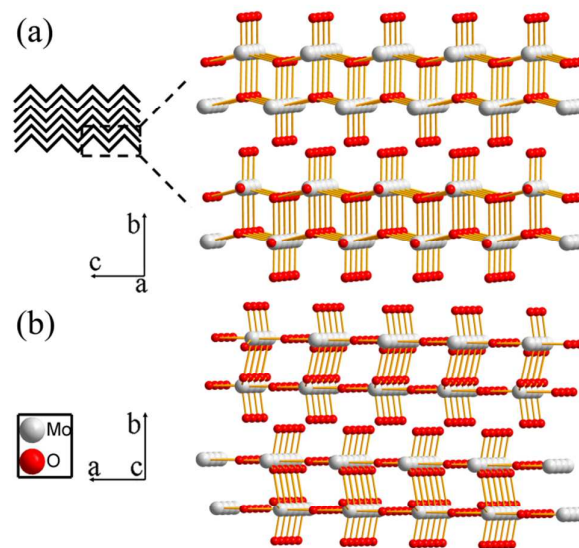


Fig. 1 Scheme structure of α-MoO₃ consisting of double layer of linked MoO₆ octahedra viewed along different axis. (a) Along [100] axis, (b) along [001] axis.

^a College of Materials Engineering, Fujian Agriculture and Forestry University, Fuzhou 350002, People's Republic of China. E-mail: qhzheng@fafu.edu.cn.

^b Fujian Institute of Research on the Structure of Matter, Chinese Academy of Sciences, Fuzhou, 350002, People's Republic of China.

for this research as it possesses a unique wide bandgap suitable for UV light detection. The bandgap of α - MoO_3 semiconductor is up to 3.2 eV,^{16, 17} corresponds to a wavelength of 388 nm, which locates at the UV spectral range. Fig.1 shows the schemes of α - MoO_3 lattice structures viewed along [100] and [001] axis. The α - MoO_3 's structure consists of double-layers of linked MoO_6 octahedra, held together by weak van der Waal's forces,^{17,18} which offers the possibility of obtaining ultra-thin 2D structures through various exfoliation methods. The absence of dangling bonds in the ultra-thin α - MoO_3 also makes it an ideal material for optoelectronic device, as the dangling bonds serve as recombination center for the photo-generated carriers.^{19, 20}

In this contribution, we demonstrate the synthesis of large scale free-standing α - MoO_3 single crystalline belt via physical vapor deposition (PVD). For the first time, we fabricate a flexible UVPD based on exfoliated MoO_3 ultra-thin nanosheet and then study its light-induced electric properties in detail. The photodetector exhibits high UV spectral selectivity, having a UV to visual rejection ratio (R380 nm/R500 nm) of over 50 times. The peak responsivity from the MoO_3 UVPD can reach as high as 183 mA W^{-1} under 380 nm UV illumination at a driving voltage of 10 V. Benefiting from the high flexibility of the 2D α - MoO_3 nanosheet, the UVPD exhibits high stability and reproducibility at different bending conditions. The UVPD also has a fast response speed that the photocurrent can be completely switched between ON and OFF states within 1 s.

Experimental

Materials and methods

The synthesis of MoO_3 free-standing belts employed a simple and facile one-step PVD by a horizon quartz tube furnace with single hot zone (Fig. S1). Briefly, the system was evacuated and maintained at 30 KPa by a mechanical pump. Argon and oxygen were introduced into the quartz tube as carrier gases with flow rates of 200 and 10 sccm, respectively. The temperature was ramped up at a rate of 5°Cmin^{-1} to a growth temperature of 950°C . Then, 1 g of the MoO_3 powder (99.5%, Huayuan Chemical Industry) on a quartz boat was inserted into the source zone by a magnetic part. After a growth time of 30 min the MoO_3 source was removed and the furnace was cooled down to room temperature naturally. Finally, a great number of large scale MoO_3 crystalline belts were dangled at the inside wall of the quartz tube at the low temperature zone. Ultra-thin MoO_3 nanosheets were prepared by mechanical exfoliation similar to the exfoliation of graphene.²¹ The mechanical exfoliation using tape (3M Scotch) was repeated 20 times, and then placed the tape on polyethylene terephthalate (PET) substrate and peeled it off.

Device fabrication

To measure the optoelectronic performances of MoO_3 nanosheet on flexible substrate, a metal-semiconductor-metal (MSM) structure photodetector based on MoO_3/PET structure was defined by a metal shadow mask. The metal electrodes

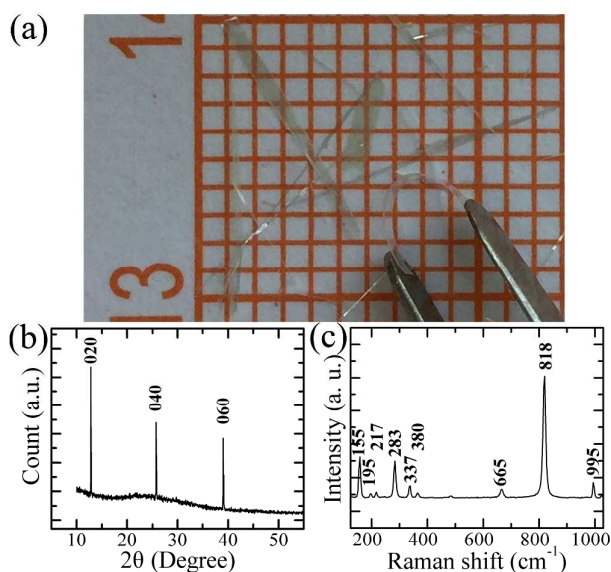


Fig. 2 (a) Photograph of large scale free-standing MoO_3 belts. (b) 0-2 θ XRD angular scan and (c) Raman spectrum of an individual MoO_3 belt.

with 30- μm gap were formed by 50 nm Au deposited via thermal evaporation. The schematic diagram of the MSM device is depicted in Fig. S2.

Characterization

The structural characterizations of the as prepared MoO_3 crystalline belts were performed with PANalytical X' Pert PRO with $\text{Cu K}\alpha$ ($\lambda = 0.15406 \text{ nm}$) source (XRD), Raman spectroscopy Horiba LabRAM HR800, scanning electron microscope Hitachi S-4800 (SEM) and transmission electron microscope JEM-2010 (TEM). Optical property was investigated using a Shimadzu UV-2501PC/2550 scanning spectrophotometer. Thickness of the MoO_3 nanosheet was measured by Bruker Dektak XT profilometer.

Current-voltage (I-V) characterizations of the fabricated UVPDs were carried out using a Keithley 2400 high resistance electrometer. The spectral responses of the UVPDs were measured using a 450 W Xe lamp and a monochromator. The monochromatic light was calibrated with a power meter LPE-1B (Phy-science Opto-electronics Co.). Time-dependent optoelectronic responses of the UVPDs were recorded by a CHI 660D work station after a pulsed excitation by a 380 nm light source (2 mWmm^{-2}) modulated by a mechanical chopper.

Results and discussion

Free-standing ultra-long MoO_3 belts with length reaching several centimeters were obtained, as shown in Fig. 2 (a). Most of these belts have typical width of 0.3~1 millimeter, and thickness ranges from several tens to several hundreds micrometers. As can be seen that individual MoO_3 belt can remain intact at the bending radius of 2 mm, revealing a high flexibility of the MoO_3 belt. The superior flexibility can be attributed to the 2D lattice structure of the crystalline belt. Fig.

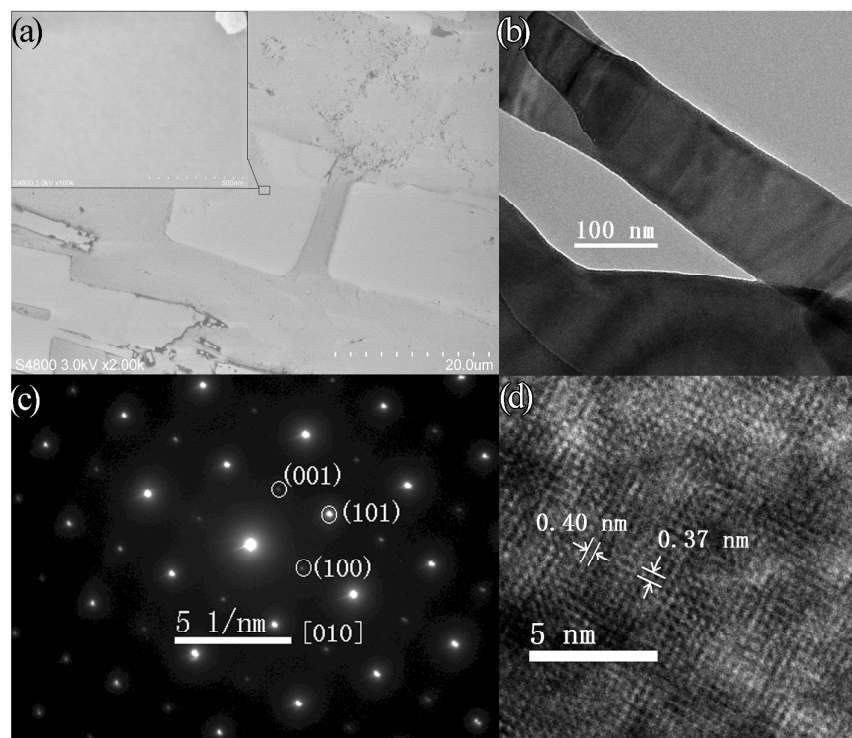


Fig. 3 (a) SEM image, (b) Medium magnification TEM image, (c) SAED pattern and (d) HRTEM image of the exfoliated MoO₃ nanosheets. The inset in (a) shows the high magnification SEM image of the dash box.

2 (b) shows the representative θ -2 θ XRD angular scan of an individual MoO₃ belt, indicating a high crystalline orthorhombic structure of the belt (JCPD file: 05-0508), as only peaks corresponding to the (020), (040) and (060) planes of orthorhombic structure could be observed. The α -MoO₃ consists of corner-sharing chains of MoO₆ octahedra that share edges with two similar chains to form layers of MoO₃ stoichiometry, as shown in Fig. 1. The adjacent layers are stacked in a staggered arrangement and held together by weak van der Waal's forces.^{17,18} The strong bond between the MoO₆ octahedra in {020} plane prevents the belt from tearing off, and the weak interaction between adjacent layers makes the belt bend freely at the direction normal to {020} plane. Thus, the 2D α -MoO₃ exhibits an excellent flexibility, which provides initial support to the feasibility of fabricating a MoO₃ based flexible photodetector.

Fig. 2 (c) presents a typical Raman spectrum of MoO₃ belts. A laser with emission wavelength centered at 532 nm was employed as the excitation source for the micro-Raman characterization. Three sharp peaks locate at 995, 818, and 665 cm⁻¹, which can be attributed to the vibration modes of α -MoO₃.²² For the crystalline α -MoO₃, the Raman bands are assigned to the terminal oxygen (Mo=O) stretching mode at 995 cm⁻¹, the triply connected bridge-oxygen (Mo₃-O) stretching mode at 665 cm⁻¹, and the doubly connected bridging oxygen (Mo₂-O) stretching mode at 818 cm⁻¹. The sharpness of the peaks demonstrates that the as-grown MoO₃ belt is highly pure with highly ordered structure. Moreover,

characteristic peaks located at 380, 337, 283, 217, 195, and 155 cm⁻¹ are also observed, which can be assigned to the bending modes of α -MoO₃.²³ The observation of characteristic results of XRD and Raman indicates that the as-grown MoO₃ belts are α -phase and have perfect crystallinity.

Due to the weak interaction between adjacent lattice planes in α -MoO₃, ultra-thin MoO₃ nanosheets can be obtained by means of mechanical exfoliation. Mechanical exfoliation effectively separates MoO₃ layers at their weakest bonds, where they are held together by weak van der Waal's forces. After exfoliation using Scotch tape for 20 times, MoO₃ ultra-thin nanosheets with thickness ranging from several nanometers to several tens of nanometers were achieved. Fig. 3 (a) shows the SEM image of the exfoliated MoO₃ ultra-thin nanosheets. The MoO₃ nanosheets have smooth surface morphology and are of high crystalline quality without showing any grain boundary.

The medium magnification TEM image in Fig. 3 (b) shows the typical morphology of the MoO₃ nanosheets with thickness of several nanometers. Fig. 3 (c) shows the select-area electron diffraction (SAED) pattern recorded with the electron beam along the [010] zone axis. The clear and symmetrical diffraction spots indicate the single-crystalline orthorhombic structure of the MoO₃ nanosheets. Periodic lattice fringes in the high resolution TEM (HRTEM) image shown in Fig. 3 (d) further confirm the single-crystal nature of the nanosheets. The lattice fringes of 0.37 nm and 0.40 nm correspond to (001) and (100) planes of α -MoO₃ crystal, respectively. TEM results

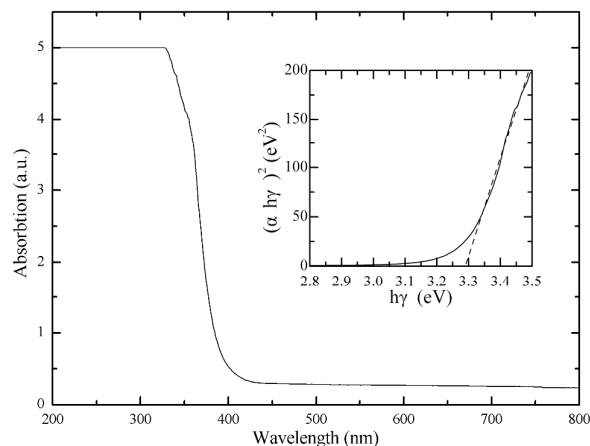


Fig. 4 UV-visible absorption spectrum of an individual MoO₃ belt. The inset shows the plot of $(\alpha hv)^2$ value of the MoO₃ belt plotted as a function of photon energy ($h\nu$).

are in agreement with data from the XRD, and we can deduce that the exfoliated nanosheets are single crystalline 2D structure with surface terminated with the {020} lattice planes. It is well known that grain boundaries and structural defects can act as recombination centers of photo-generated carriers and paths of leakage current in the optoelectronic devices. As a result, the good crystalline quality of the obtained MoO₃ nanosheets can help to fabricate UVPDs with high responsivity

and low dark current.

The as-synthesized MoO₃ belts shown in Fig. 2 (a) are colorless and highly transparent. Fig. 4 shows the UV-visible absorption spectrum of an individual MoO₃ belts. As can be seen, MoO₃ belt absorbs strongly only in the UV region and is highly transparent for visible light, while a sharp absorption edge exhibits at around 380 nm. As a crystalline semiconductor, the optical absorption near the band edge obeys the formula,²⁴

$$(\alpha hv)^2 = A(h\nu - E_g) \quad (1)$$

where α , h , ν , A and E_g are the absorption coefficient, planck's constant, incident photon frequency, a constant and bandgap, respectively. The bandgap of the MoO₃ belt is derived from a plot of $(\alpha hv)^2$ as a function of photon energy ($h\nu$) and evaluated to be 3.28 eV, as shown in the inset. The bandgap is very close to the values for α -MoO₃ nanoribbon (3.18 eV) and thin film (3.26 eV).^{25, 26} The UV-Visible absorption results suggest that optical properties of α -MoO₃ material are suitable for UVPD application. Moreover, compared with narrow bandgap semiconductor, wide bandgap semiconductor devices are capable of much higher temperature operation and reducing the junction leakage current by at least several orders of magnitude.^{27, 28}

The inset of Fig. 5 (a) shows an optical microscope image of MSM structure device based on 78.4 nm MoO₃ nanosheet transferred to PET substrate, with an electrode channel of 30 μ m. In such structure, both contacts form Schottky barriers and the externally applied voltage is mainly dropped across

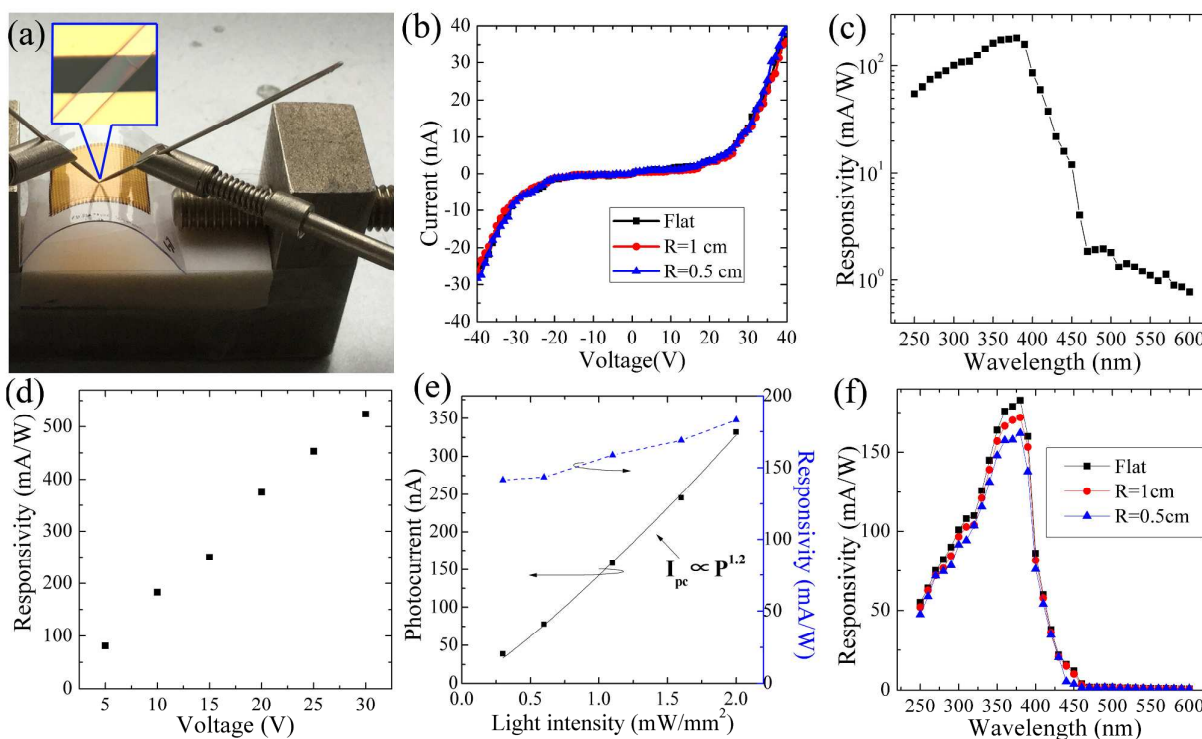


Fig. 5 (a) Photograph of wafer-scale MoO₃ nanosheet devices measured at bending condition. The inset shows the optical microscope image of MSM structure device. (b) Dark I-V characteristics measured under different bending conditions. (c) Spectral responsivity $R(\lambda)$ characteristics at 10 V. (d) Maximum responsivity versus bias voltage. (e) Peak photocurrent and maximum responsivity as function of illumination density at 10 V. (f) Spectral responsivity $R(\lambda)$ characteristics under different bending conditions.

the reverse-biased electrode. Flexible optoelectronics are easily subjected to a variety of mechanical deformations that may degrade their performance, such as bending, compression, and tension. To investigate the mechanical stability of the device, optoelectronic performances under flat and bending conditions were compared systematically. Fig. 5 (a) presents the photograph of wafer-scale flexible MoO₃ nanosheet devices measured with a bending radius of 1 cm.

Fig. 5(b) shows the dark I-V curves of photodetector measured under flat and bending (with bending radius of 1 and 0.5 cm conditions, respectively). After bending, there are no obvious changes in the dark IV characteristics, which can be attributed to the high flexibility of the 2D MoO₃ nanosheet and good metal contact of the device. The nonlinear behaviors and double diode-like characteristics of dark I-V characteristic originate from the formation of double Schottky contacts between the MoO₃ nanosheet and the Au electrodes. The dark current is only 0.9 nA at 10V and below 10 nA with bias ranging from -20V to 20V.

Table 1 summarizes earlier reports on flexible UVPDs and visible photodetectors based on other 2D nanostructures. A comparison to typical rigid UVPDs based on ZnO nanostructures is also made. As compared to the photodetectors based on semiconductors with narrow bandgap,^{12, 15, 29} our UVPD possess much lower dark current. The low dark current should be attributed to the wide bandgap, high crystalline quality of the MoO₃ nanosheet and Schottky barrier between the MoO₃ nanosheet and Au electrodes. A low dark current is help to obtain photodetector with small power consumption and low system noise.

Fig. 5 (c) represents spectral responsivity $R(\lambda)$ characteristics of the flexible photodetector to the light of different wavelengths, at an applied voltage of 10 V. The photodetector shows a highest selectivity to 380 nm light with a cutoff wavelength of around 400 nm, which is consistent with the absorption result of the MoO₃. The UV/Visible rejection ratio ($R_{380\text{ nm}}/R_{500\text{ nm}}$) is over 50 times, suggesting a high UV sensitivity of the MoO₃ based photodetector. The peak responsivity reaches a value of 183 mA W⁻¹. The peak responsivity further increases with increasing applied bias, as shown in Fig. 5 (d), indicating no carrier

mobility saturation or sweep-out effect up to the applied bias.³³ At an applied voltage of 30 V, the peak responsivity is as high as 524 mA W⁻¹, which corresponds to total quantum efficiency of 171%. The photoresponse performance is better than several other reported flexible UVPDs,^{9, 30, 31} and visible photodetectors based on other 2D nanosheets,^{12, 29} as also listed in table 1. The high responsivity is realized mainly by high carrier mobility in the 2D lattice structure and long lifetime of photo-generated carriers in highly crystallized MoO₃ nanosheet.

Fig. 5 (e) shows the photocurrent and responsivity of the UVPD illuminated by 380 nm light with the intensity varying from 0.3 to 2.0 mWmm⁻² at a fixed bias of 10 V. As the photo-generated carriers are proportional to the absorbed photon flux, the photocurrent increases with the increasing light intensity. It was found that the photocurrent (I_{pc}) can be fitted well to a simple power law $I_{pc} \propto P^{1.2}$, where P is the power of illumination.³⁴ The non-unity exponent can be attributed to the complex process of electron-hole generation, trapping and recombination within the MoO₃ nanosheet.³⁴ Accordingly, the responsivity of the MoO₃ UVPD increases slightly with the increasing light intensity, as also shown in Fig. 5 (e).

The spectral responsivity $R(\lambda)$ characteristics of the UVPD under different bending conditions are compared in Fig. 5 (f). Independent of the bending, the response spectrums remain stable without showing obvious red shift or blue shift. The responsivity of the MoO₃ UVPD decreases slightly with the increasing degree of bending, in agreement with the decrease in effective irradiance. The stable device characteristics can be attributed to the high crystalline quality of the MoO₃ nanosheet and high flexibility of the 2D lattice structure. These results demonstrate that our flexible MoO₃ based UVPD is able to bear certain mechanical deformations.

Fig. 6(a) shows the time dependent photo-electronic response of the MoO₃ UVPD measured with 5 s periodic illumination of 380 nm UV light (2mWmm⁻²). Under UV illumination, photocurrent increases to stable value, and then decreases to its initial value as the light was turned off, exhibiting good stability and reproducible characteristics. At an applied voltage of 10 V, the photocurrent dramatically increases from 0.9 nA in the dark to 331.8 nA upon UV

Table 1 Comparison of device characteristics of this work and photodetectors based on other nanostructures.

Material	Flexible	Spectral	Dark current	Responsivity	Response time	Ref.
MoO ₃ Nanosheet	Yes	UV	0.9 nA/10 V	524 mA W ⁻¹	0.94 s	This work
Zn ₂ GeO ₄ Nanowires	Yes	UV	10 fA/10 V	—	2.6 s	9
In ₂ Ge ₂ O ₇ Nanowires	Yes	UV	0.05 nA/15 V	—	15 s	30
SnO ₂ nanospheres	Yes	UV	7.3 pA/5 V	—	>30 s	31
WS ₂ Multilayer	No	VIS	20 μA/20 V	92 μA W ⁻¹	5.3 ms	12
MoS ₂ Multilayer	No	VIS	35 nA/1 V	120 mA W ⁻¹	—	29
GaSe Few-layers	No	UV-VIS	1 nA/1V	2.8 A W ⁻¹	20 ms	15
CuSCN-ZnO nanowire	No	UV	—	7.5 mA W ⁻¹	6.7 μs	6
ZnO Nanotetrapod	No	UV	1 nA/0.3 V	—	30 ms	32
Graphene-ZnO nanorod	No	UV	—	3×10 ⁵ A W ⁻¹	1.9 s	7

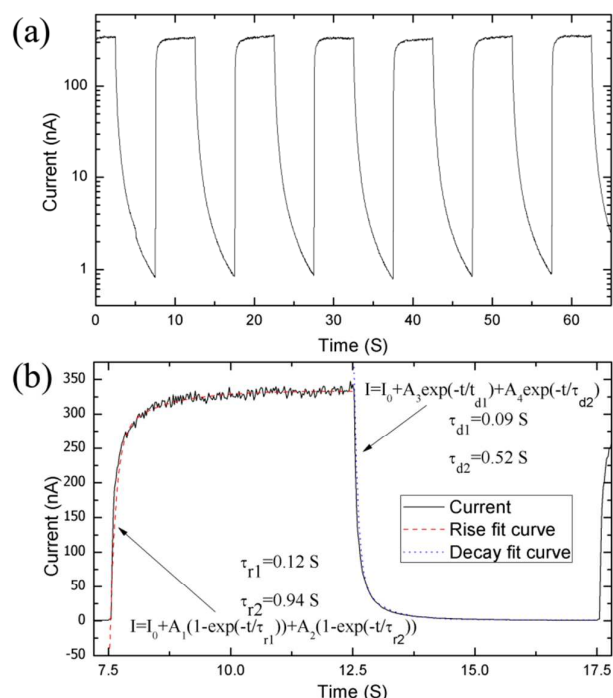


Fig. 6 (a) Time response of the MoO₃ UVPD obtained using 380 nm monochromatic light pulses with 5 s duration at 10 V bias. (b) The rise and decay of the current in a single pulse response cycle. The red and blue lines represent the bi-exponential fitting results of the rising and falling edges, respectively.

illumination, showing a high UV sensitivity with on/off switching ratio of over two orders.

Fig. 6(b) gives a single time-dependent on/off cycle of the device. The MoO₃ UVPD is found to exhibit a fast response time to UV light irradiation. The rise and decay photocurrents follow exponential function, which can be fitted by bi-exponential function equation:³²

$$I = I_0 + A_1(1 - \exp(-t/\tau_{r1})) + A_2(1 - \exp(-t/\tau_{r2})) \quad (2)$$

$$I = I_0 + A_3 \exp(-t/\tau_{d1}) + A_4 \exp(-t/\tau_{d2}) \quad (3)$$

where I_0 is dark current, A_1 , A_2 , A_3 and A_4 are positive constants. τ_{r1} , τ_{r2} are the first and second rise time constant, and τ_{d1} , τ_{d2} are the first and second decay time constants, respectively. On the basis of the curve fittings, the rise time constants are $\tau_{r1} = 0.12$ s and $\tau_{r2} = 0.94$ s, while the decay time constants are $\tau_{d1} = 0.09$ s and $\tau_{d2} = 0.52$ s, respectively.

Admittedly, the response time from our MoO₃ UVPD is long as compared to the reported UVPD based on ZnO/CuSCN nanowires heterojunction (6.7 μ s) or that based on ZnO Nanotetrapod (30 ms),^{6, 11} but it is shorter than many typical flexible UVPDs that based on Zn₂GeO₄ Nanowires (2.6 s),⁹ In₂Ge₂O₇ Nanowires (15 s),³⁰ and SnO₂ nanospheres (>30 s),³¹ as also listed in table 1. The relative lower response speed in flexible photodetector is probably due to the existence of dense interface states between the semiconductor and PET substrate, which can trap photo-generated carriers and lead to a long life time of the carriers. The oxygen

absorption/desorption processes at the surface of the nanostructures would further prolong the response time of the flexible UVPD based on nanoparticles and nanowires.³⁵ Compared to nanoparticles and nanowires, the aspect ratio of 2D nanosheets is relative smaller, result in a higher response speed of the MoO₃ nanosheets based UVPD. Moreover, the high carrier mobility in the 2D lattice structure can decrease the drift time of the photo-generated carriers between the Au electrodes and further improve the response speed of our UVPD. Both rise and decay time constants of the fabricated MoO₃ UVPD are within 1 s, allowing the device to act as a high speed UV photosensitive switch.

Conclusions

In this work, we obtained centimeter-scale high crystalline α -MoO₃ belts through a simple PVD-grown method. The fabrication of flexible UVPDs was accomplished based on the exfoliated nanosheets transferred onto PET substrate. Due to its relatively wide bandgap of 3.28 eV, MoO₃ nanosheet can potentially be integrated into various optical sensors that require a UV spectral response, as an alternative to the conventional GaN and ZnO based UVPDs. The UVPD exhibits excellent operating characteristics, including a high responsivity of 183 mA W⁻¹, a high on/off ratio of over two orders, a response speed of below 1 s and high optoelectronic stability (i.e., no-shift in the spectral response) under mechanical deformations. MoO₃ flexible UVPD can be attractive for a variety of industrial applications, such as wearable UV meter, touch sensor panels, communication devices and UV image camera.

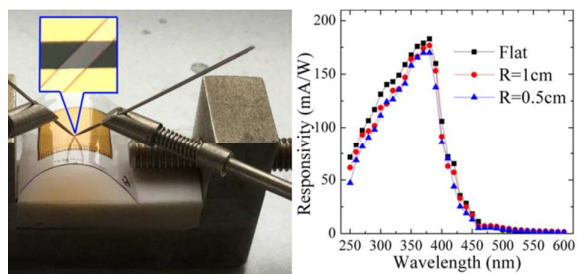
Acknowledgements

The authors would like to acknowledge the funding support from the National Natural Science Foundation of China (61306065, 31270638 and 11404057) and Natural Science Foundation of Fujian Province (J).

Notes and references

- L. Shi, F. Wang, B. Li, X. Chen, B. Yao, D. Zhao and D. Shen, *J. Mater. Chem. C*, 2014, **2**, 5005-5010.
- M.-M. Fan, K.-W. Liu, X. Chen, Z.-Z. Zhang, B.-H. Li, H.-F. Zhao and D.-Z. Shen, *J. Mater. Chem. C*, 2015, **3**, 313-317.
- Q. H. Zheng, F. Huang, J. Huang, H. Q. C., D. G. Chen and K. Ding, *IEEE Electron Device Lett.*, 2012, **33**, 1033-1035.
- X. Fang, Y. Bando, M. Liao, U. K. Gautam, C. Zhi, B. Dierre, B. Liu, T. Zhai, T. Sekiguchi, Y. Koide and D. Golberg, *Adv. Mater.*, 2009, **21**, 2034-2039.
- J. Yang, F. Lu, Y. Li, S. Yang, R. Li, N. Huo, C. Fan, Z. Wei, J. Li and S.-S. Li, *J. Mater. Chem. C*, 2014, **2**, 1034-1040.
- S. M. Hatch, J. Briscoe and S. Dunn, *Adv. Mater.*, 2013, **25**, 867-871.
- V. Q. Dang, T. Q. Trung, D. I. Kim, L. T. Duy, B. U. Hwang, D. W. Lee, B. Y. Kim, L. D. Toan and N. E. Lee, *Small*, 2015, DOI: 10.1002/sml.201403625.

8. G. Yu, Z. Liu, X. Xie, X. Ouyang and G. Shen, *J. Mater. Chem. C*, 2014, **2**, 6104-6110.
9. J. Wang, C. Yan, M.-F. Lin, K. Tsukagoshi and P. S. Lee, *J. Mater. Chem. C*, 2015, **3**, 596-600.
10. Z. Gao, W. Jin, Y. Zhou, Y. Dai, B. Yu, C. Liu, W. Xu, Y. Li, H. Peng, Z. Liu and L. Dai, *Nanoscale*, 2013, **5**, 5576-5581.
11. P. Hu, L. Wang, M. Yoon, J. Zhang, W. Feng, X. Wang, Z. Wen, J. C. Idrobo, Y. Miyamoto, D. B. Geohegan and K. Xiao, *Nano Lett.*, 2013, **13**, 1649-1654.
12. N. Perea-López, A. L. Elías, A. Berkdemir, A. Castro-Beltran, H. R. Gutiérrez, S. Feng, R. Lv, T. Hayashi, F. López-Urías, S. Ghosh, B. Muchharla, S. Talapatra, H. Terrones and M. Terrones, *Adv. Funct. Mater.*, 2013, **23**, 5511-5517.
13. Z. Yin, H. Li, H. Li, L. Jiang, Y. Shi, Y. Sun, G. Lu, Q. Zhang, X. Chen and H. Zhang, *Acs Nano*, 2011, **6**, 74-80.
14. G. Cunningham, U. Khan, C. Backes, D. Hanlon, D. McCloskey, J. F. Donegan and J. N. Coleman, *J. Mater. Chem. C*, 2013, **1**, 6899-6904.
15. P. Hu, Z. Wen, L. Wang, P. Tan and K. Xiao, *Acs Nano*, 2012, **6**, 5988-5994.
16. D. Xiang, C. Han, J. Zhang and W. Chen, *Sci Rep-Uk*, 2014, **4**, 4891.
17. S. Balendhran, J. Deng, J. Z. Ou, S. Walia, J. Scott, J. Tang, K. L. Wang, M. R. Field, S. Russo and S. Zhuiykov, *Adv. Mater.*, 2013, **25**, 109-114.
18. K. Kalantar-zadeh, J. Tang, M. Wang, K. L. Wang, A. Shailos, K. Galatsis, R. Kojima, V. Strong, A. Lech, W. Wlodarski and R. B. Kaner, *Nanoscale*, 2010, **2**, 429.
19. S. Olibet, E. Vallat-Sauvain and C. Ballif, *Phys. Rev. B*, 2007, **76**, 035326.
20. F. Vaillant and D. Jousse, *Physical Review B*, 1986, **34**, 4088.
21. K. S. Novoselov, A. K. Geim, S. Morozov, D. Jiang, Y. Zhang, S. Dubonos, I. Grigorieva and A. Firsov, *science*, 2004, **306**, 666-669.
22. T. He and J. Yao, *Journal of Photochemistry and Photobiology C: Photochemistry Reviews*, 2003, **4**, 125-143.
23. K.-K. Wang, F.-X. Wang, Y.-D. Liu and G.-B. Pan, *Mater. Lett.*, 2013, **102-103**, 8-11.
24. M. Butler, *J. Appl. Phys.*, 1977, **48**, 1914-1920.
25. L. Cheng, M. Shao, X. Wang and H. Hu, *Chem. Eur. J.*, 2009, **15**, 2310-2316.
26. T. S. Sian and G. B. Reddy, *Sol. Energy Mater. Sol. Cells*, 2004, **82**, 375-386.
27. P. G. Neudeck, R. S. Okojie and L.-Y. Chen, *P IEEE*, 2002, **90**, 1065-1076.
28. E. Monroy, F. Omnès and F. Calle, *Semicond. Sci. Technol.*, 2003, **18**, R33-R51.
29. W. Choi, M. Y. Cho, A. Konar, J. H. Lee, G. B. Cha, S. C. Hong, S. Kim, J. Kim, D. Jena and J. Joo, *Adv. Mater.*, 2012, **24**, 5832-5836.
30. Z. Liu, H. Huang, B. Liang, X. Wang, Z. Wang, D. Chen and G. Shen, *Opt. Express*, 2012, **20**, 2982-2991.
31. W. Tian, C. Zhang, T. Zhai, S.-L. Li, X. Wang, M. Liao, K. Tsukagoshi, D. Golberg and Y. Bando, *Chem. Commun.*, 2013, **49**, 3739-3741.
32. D. Gedamu, I. Paulowicz, S. Kaps, O. Lupan, S. Wille, G. Haidarschin, Y. K. Mishra and R. Adelung, *Adv. Mater.*, 2014, **26**, 1541-1550.
33. Q. Zheng, F. Huang, K. Ding, J. Huang, D. Chen, Z. Zhan and Z. Lin, *Appl. Phys. Lett.*, 2011, **98**, 221112.
34. H. Kind, H. Yan, B. Messer, M. Law and P. Yang, *Adv. Mater.*, 2002, **14**, 158.
35. X. Fang, Y. Bando, M. Liao, T. Zhai, U. K. Gautam, L. Li, Y. Koide and D. Golberg, *Adv. Funct. Mater.*, 2010, **20**, 500-508.



Flexible UV photodetector was fabricated based on high crystalline MoO_3 nanosheet. The photodetector exhibits high UV spectral selectivity, excellent stability, fast response speed and is able to bear significant external mechanical forces.